scientific reports

Check for updates

OPEN

Atomic force microscopy reveals morphological and mechanical properties of *schistosoma mansoni* tegument

Adriane M. C. Dantas[1], Fernanda S. Teixeira[1], Raissa L. Oblitas[1], Wagner W. R. Araújo[1], Monique C. Amaro[2], Rayssa A. Cajas[2], Josué de Moraes[2,3]✉ & Maria C. Salvadori[1]✉

***Schistosoma mansoni*, an intravascular parasitic worm and the causative agent of schistosomiasis, relies on its tegument (outer layer) for survival and host interaction. This study explored the morphology and mechanical properties of *S. mansoni* tegument using Atomic Force Microscopy (AFM). Notably, we employed the PeakForce Quantitative Nanomechanical Mapping (PF-QNM) mode in air, enabling simultaneous acquisition of 3D topography and mechanical property contrasts (adhesion, elastic modulus). Additionally, nanoindentation (AFM contact mode) was performed on female worm tegument for elastic modulus measurement. Both techniques revealed an elastic modulus range of fractions or units of GPa for the tegument. Interestingly, mechanical property maps, particularly adhesion contrast, displayed a recurring pattern of light and dark bands. We also measured the depth of annular furrows on the female tegument, finding an average of 128 ± 10 nm. These findings establish AFM, particularly PF-QNM, as a valuable tool to characterize *S. mansoni* tegument properties, offering insights for future investigations into parasite biology and its response to immunological or pharmacological challenges.**

Schistosomiasis stands as one of the most significant parasitic diseases globally, deemed a neglected ailment by the World Health Organization (WHO). Endemic in 78 countries, it affects approximately 250 million individuals, predominantly those residing in impoverished communities deprived of basic sanitation, thus exacerbating social inequality and hindering national development[1]. Despite its significance, schistosomiasis currently relies solely on praziquantel for treatment and control[2,3]. However, while praziquantel effectively reduces morbidity, its outcomes have fallen short of expectations[4–6], with concerns emerging regarding drug resistance and its inefficacy against young parasite forms[2,7].

Schistosoma mansoni (*S. mansoni*), an intravascular parasitic flatworm, is one of the main species responsible for human schistosomiasis. It is found in over 50 countries across the American and African continents[8]. The parasite goes through different phases and lives in diverse hosts and environments, with a prominent capacity for adaptation and multiplication. These parasites carry out an asexual cycle in molluscs of the genus *Biomphalaria*, while adult specimens carry out a sexual cycle and are found in the mesenteric vessels and portal system of mammals, especially humans[9,10]. Females can produce hundreds of eggs daily, with many exiting the host through feces, while others become lodged in the liver and other tissues permanently. *S. mansoni* infection is predominantly intestinal, typically presenting mild symptoms; however, severe cases may lead to hepatosplenomegaly and periportal fibrosis[11].

The tegument (skin) of schistosomes plays a vital role in protecting the worms, facilitating interaction with the host, and ensuring parasite survival. In the literature, *S. mansoni* has been widely characterized using various techniques, including optical microscopy[12–14], fluorescence microscopy[15], confocal laser scanning microscopy[16,17], transmission electron microscopy[18] and scanning electron microscopy (SEM)[12–14,19,20]. However, to date, only a few studies have reported on its characterization using Atomic Force Microscopy (AFM), primarily focusing on morphology[21].

The AFM technique was developed by Binning et al. in 1986[22]. It serves as a highly powerful tool for acquiring morphological images and gathering information about mechanical properties at the nanometric

[1]Instituto de Física, Universidade de São Paulo, São Paulo 05508090, SP, Brazil. [2]Núcleo de Pesquisas em Doenças Negligenciadas, Universidade Guarulhos, Guarulhos 07023-070, SP, Brazil. [3]Núcleo de Pesquisas em Doenças Negligenciadas, Instituto Científico e Tecnológico, Universidade Brasil, São Paulo 08230-030, SP, Brazil. ✉email: moraesnpdn@gmail.com; mcsalva@if.usp.br

scale, such as elastic modulus and adhesiveness. This technique enables characterization of various materials, including biological specimens like cells[23,24], hair fibers[25] and nematodes[26]. The characterization of *S. mansoni* by AFM holds significance as it allows for analyzing the mechanical properties of this worm, providing a deeper understanding of its morphological features. These insights have implications for parasite biology and survival under immunological or pharmacological pressure, paving the way for further exploration in the field.

This study aims to characterize the tegument of *S. mansoni* helminth using AFM, assessing both its morphology and mechanical properties. We employed the PeakForce Quantitative Nanomechanical Mapping (PF-QNM)[27] operating mode and array force curve (AFC) in AFM contact mode, novel approaches not previously explored in the literature for this purpose. The PF-QNM mode generates maps of mechanical properties, such as elastic modulus and adhesion between the tip and the sample, alongside the three-dimensional topographic image of the surface under analysis, achieved through nanoindentation measurements.

Results and discussion

Initially, the tegument of both male and female *S. mansoni* adult worms was examined using SEM (Fig. 1). Morphological disparities between the teguments of male and female parasites are evident: males exhibit tubercles encircled by spicules, whereas the tegument of female worms appears predominantly flat, with shallow furrows. For SEM analysis, samples are conventionally coated with a thin layer of gold[28].

For AFM analysis, initially, the *S. mansoni* helminth of both sexes were characterized by PF-QNM technique without tip calibration, analyzing only the contrasts in the images of mechanical properties. Following, PF-QNM images (after tip calibration) were performed for female worms. Note that, when it comes to topography, we will always have the x y and z coordinates in absolute values; but, regarding mechanical properties, absolute values will only be obtained after calibrating the tip. When there is no tip calibration, the mechanical property contrasts are still valid.

The elastic modulus of the female worm tegument was obtained using the Sneddon model, utilizing data from PF-QNM and AFC, as will be detailed in Methods. However, a necessary condition for applying the Sneddon model is that the ratio between the adhesion force and the maximum applied force must be small. As observed

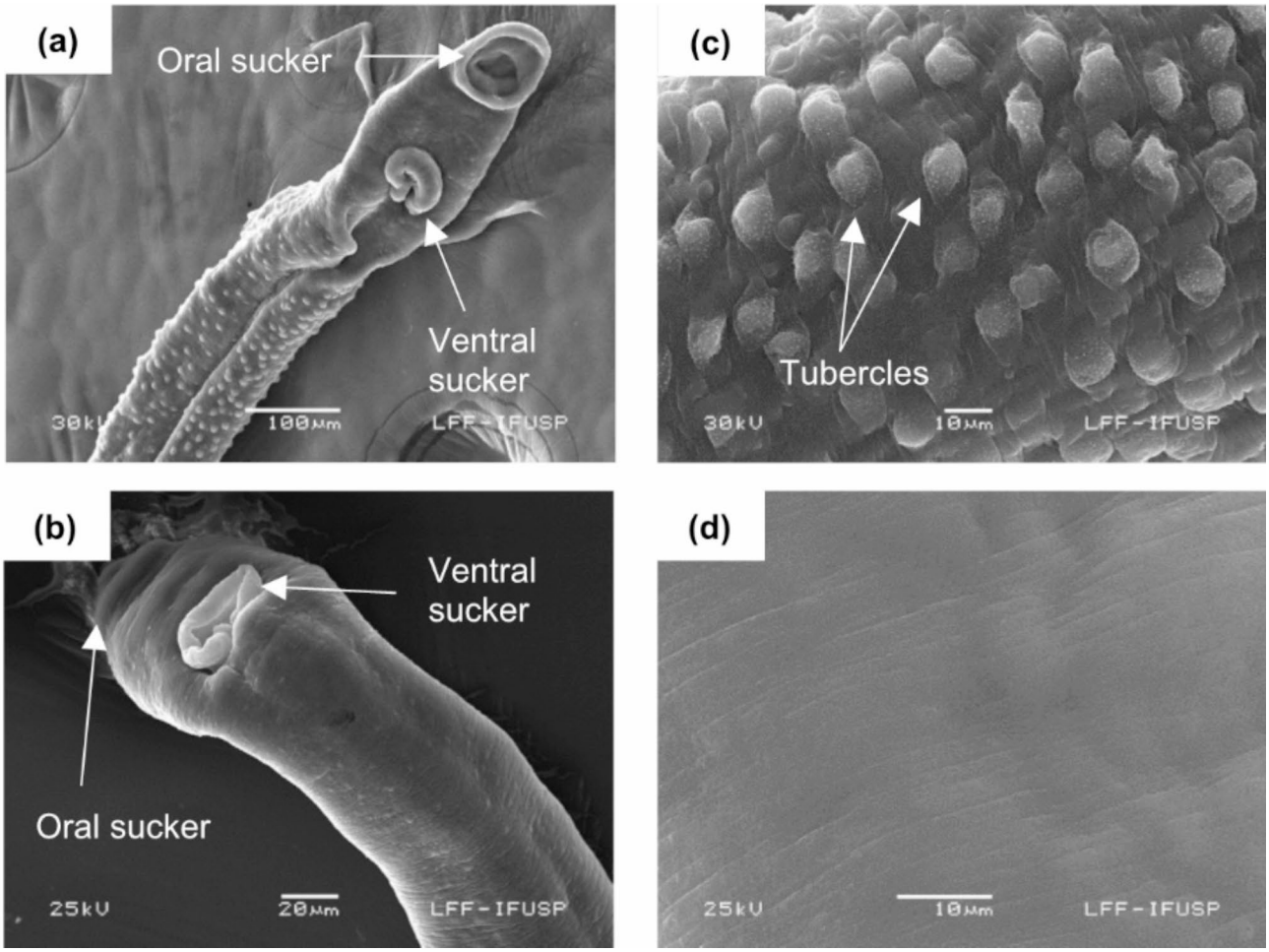

Fig. 1. Representative images of *Schistosoma mansoni* helminths highlighting some characteristics, such as the oral and ventral suckers of the male **(a)** and female **(b)** helminth, and characteristics of their teguments **(c)** and **(d)**, respectively.

in Fig. 2, this ratio is less than 0.1, for each region analyzed and by both methods, by PF-QNM and by AFC. Therefore, Sneddon model can be applied to our data[25].

Peakforce quantitative nanomechanical mapping (PF-QNM) imaging

The PF-QNM operating mode of AFM in air was used to characterize the tegument of the *S. mansoni* helminth regarding its topography and contrasts of corresponding mechanical properties, such as elastic modulus and adhesiveness, initially without tip calibration, with a resolution of 512 × 512 pixels. Figure 3 shows two PF-QNM images of the body central region of two different female worms with the respective images with adhesion and elastic modulus contrasts, the last adjusted to the DMT model. On the color scale, regions with lighter intensities mean higher values of the corresponding property. In the topography (Height) image in Fig. 3a, it is possible to observe furrows indicated by black arrows. In the images with adhesion contrast in Fig. 3, we observed a pattern composed by light and dark bands (fringes). These fringes are present in 53% of the images with adhesiveness contrasts in 202 PF-QNM image acquisitions of 36 female worms, and in 7% of the images the fringes are also present in the elastic modulus image, as seen more prominently in Fig. 3b. Images with different scan sizes obtained from regions presenting this fringe pattern reproduced the pattern according to the magnification, attesting that it is not an artifact[29]. The spatial period of this fringe pattern was measured in the images using the "cross section" tool available in the NanoScope Analysis 1.5 software, analyzing the spectral period of a line drawn perpendicular to the direction of the fringes. The average of spatial period of the fringes was (715 ± 37) nm (mean ± standard error on the mean). These measurements were carried out on 33 adhesive contrast images of 14 female worms, with a scan size of 10 µm.

The furrows present in the tegument of female helminths are important for nutrient absorption and oviposition[30]. The depth of these furrows was measured using the "cross section" tool available in the NanoScope Analysis 1.5 software, measuring the peak-valley distance. The measurement was carried out from 33 images with scan size of 10 µm, taken from 14 worms. The depth histogram is shown in Fig. 4. An average value of (128 ± 10) nm (mean ± standard error on the mean) was obtained.

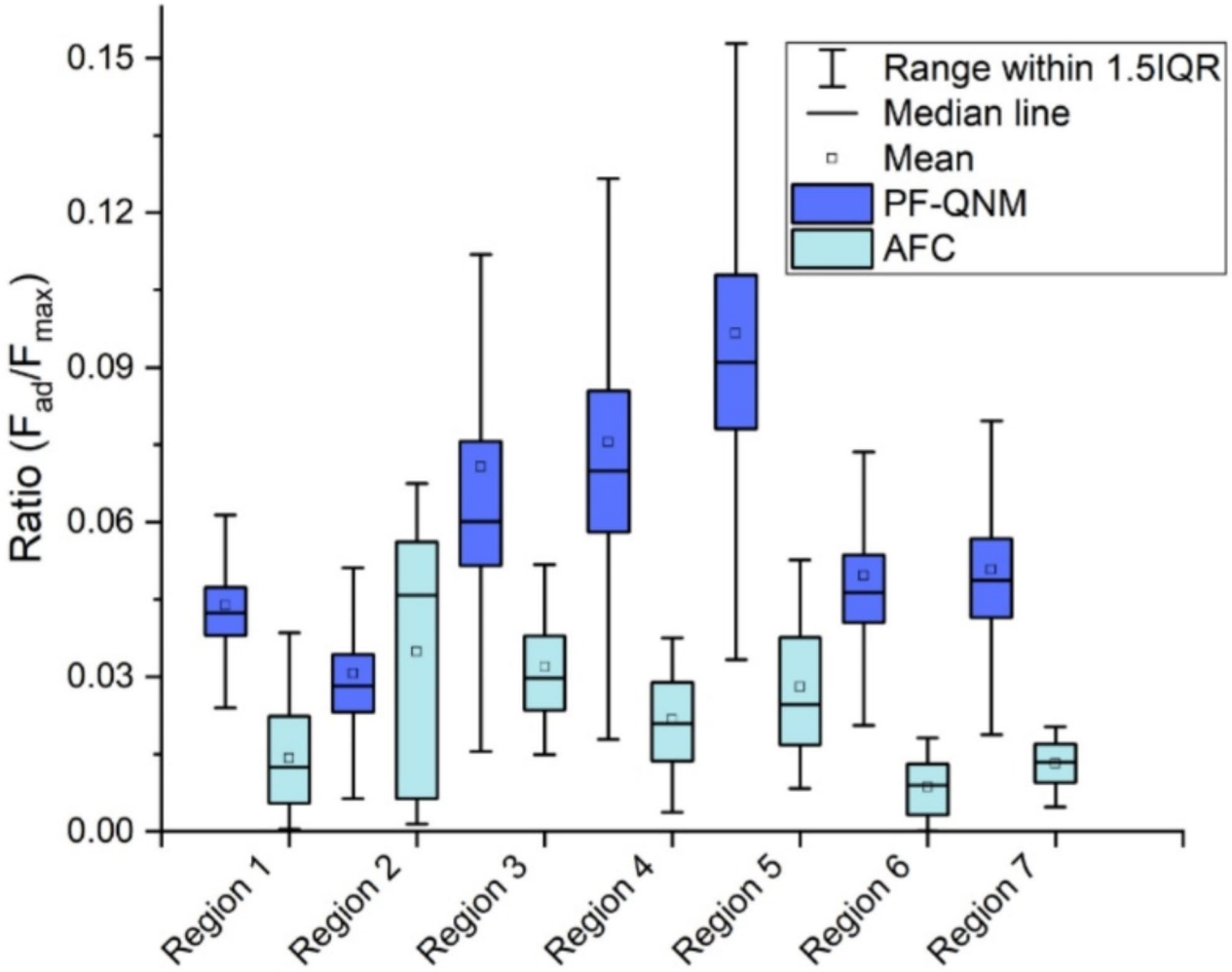

Fig. 2. Ratio between the adhesion force F_{ad} and the maximum force F_{max} exerted by the tip on the sample for data obtained using PF-QNM and AFC.

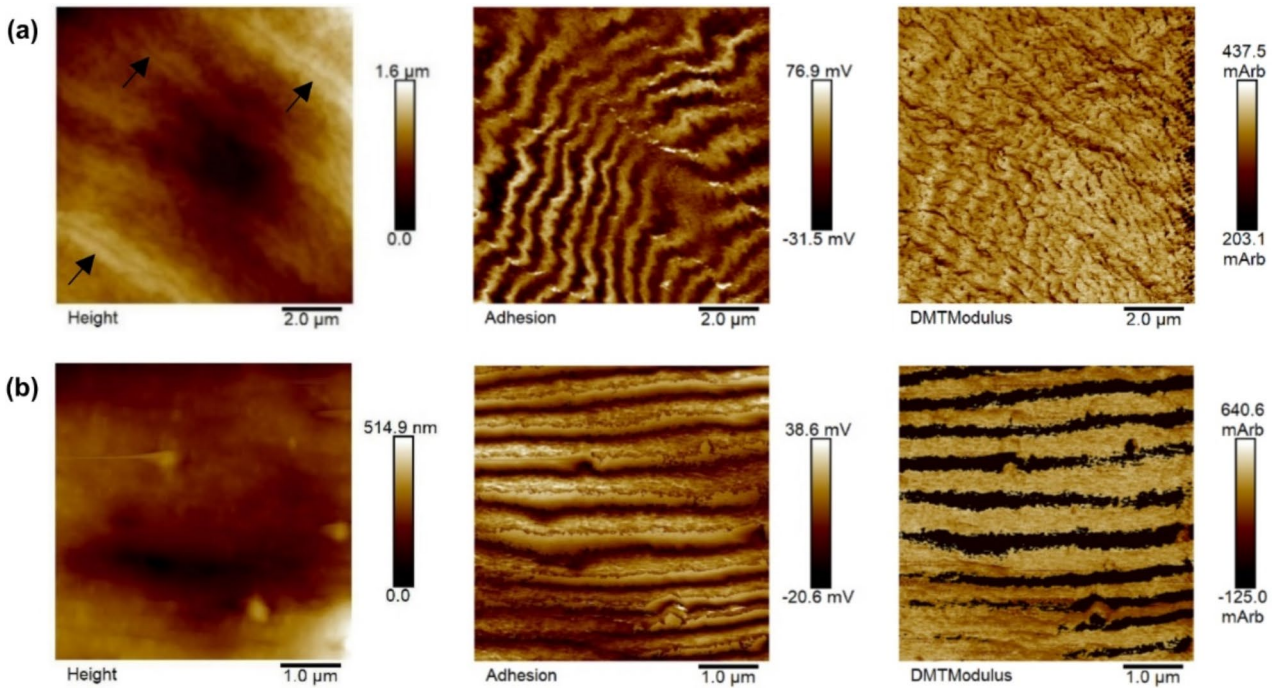

Fig. 3. Images **(a)** and **(b)** depict PF-QNM images in air of female *S. mansoni* helminths, illustrating the topographic image (Height) with their respective adhesion contrast and elastic modulus (DMTModulus) maps. The arrows in the height image of **(a)** indicate some furrows present in the region.

AFM analysis was also performed to investigate the surface topography, adhesion properties, and elastic modulus of male *S. mansoni* worms. Representative topography images (Fig. 5a) revealed the presence of tubercles with visible spicules on one side and smooth regions devoid of structures on the other. Valleys were also observed in another microregion (Fig. 5b and c). Analysis of adhesion contrast images (Fig. 5) showed a recurring fringe pattern similar to that observed in female worms. This pattern intensified with increasing magnification, suggesting it's an intrinsic property of the sample surface. Notably, these fringes typically surrounded areas of unevenness, such as valleys and protuberances. Interestingly, fringe patterns were present in 57% of the male worm adhesion images analyzed. Finally, based on the corresponding elastic modulus contrast image, the region with the highest concentration of spicules in Fig. 5a appears to have the highest elastic modulus.

A detailed analysis of the region between the oral and ventral suckers of a male worm is provided by the AFM PF-QNM image in Fig. 5d. The topography reveals the presence of furrows, while the corresponding adhesion image shows peaks in these same regions. This suggests that the internal tissue exposed by the furrows exhibits greater adhesiveness compared to the external tegument of the worm. The elastic modulus image displays slightly lighter shades at the edges of the furrows, potentially indicating a slightly higher elastic modulus in these areas.

Elastic modulus determination

Female worms were analyzed by PF-QNM images after tip calibration with a resolution of 256×256 pixels, resulting in 65,536 force curves (FC) per image. PF-QNM representative images of male *S. mansoni* helminth is shown in Fig. 6a, regarding topography, adhesion contrast and elastic modulus fitted to Sneddon model. Seven images were acquired in regions of the anterior half of each female worm. Two of these images are presented in Fig. 6b. In the same regions, arrays of force curves (AFC) were carried out, in the AFM contact mode. The raw force curves obtained by both techniques (PF-QNM and AFC) were processed by Atomic J 2.3.1 software[31] using the Sneddon model. The natural logarithm histograms of the elastic modulus (ln(*E*)) in the regions presented in Fig. 6b are given in pairs (PF-QNM and AFC) in Fig. 6c. The upper scale in Fig. 6c corresponds to the elastic modulus value in GPa.

Table 1 summarizes the average elastic modulus values and R^2 statistics obtained for the seven analyzed regions of female *S. mansoni* worms using both PF-QNM and AFC techniques. All regions were analyzed with 65,536 FCs for PF-QNM, and 25 FCs for AFC (except region 1 with 100 FCs for AFC). The data indicate that the elastic modulus of the schistosomes tegument ranges from 0.2 to 3.4 GPa. The reference[32] presents the elastic modulus of one of the worm stages (*Haemonchus contortus*), resulting in about 0.2 GPa, that is the same order of magnitude of our results. Note that, the elastic modulus measurement can be affected by the biological material fixation, related to biological material in life, the same can be claimed concerning to dry or wet environment. But we added in this article a supplementary material where we show that, using AFA and applying different concentrations of praziquantel in *S. mansoni*, the elastic modulus was affected, increasing with the increase the praziquantel concentration. This justifies the choose of elastic modulus as an important parameter, using AFA.

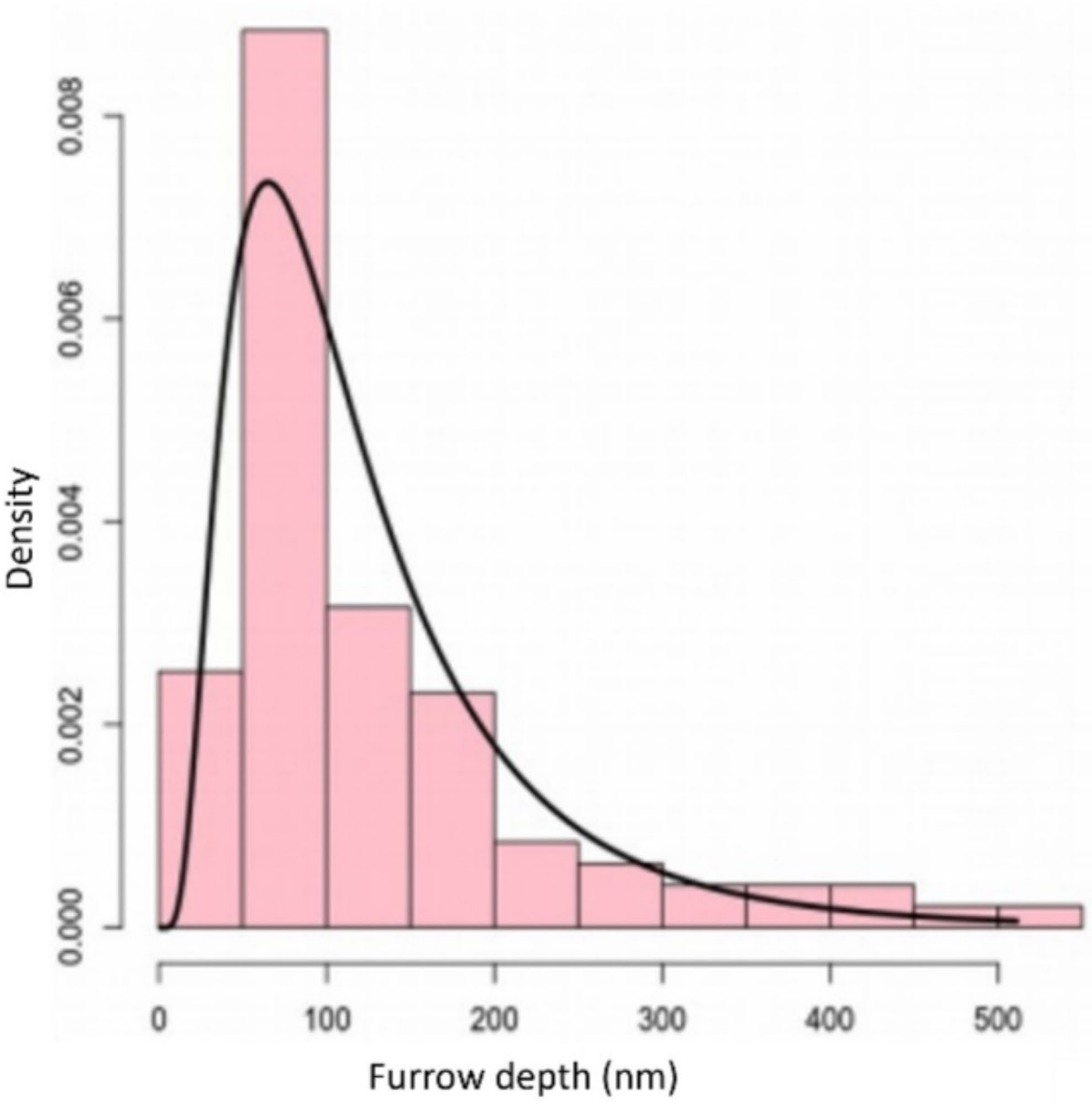

Fig. 4. Histogram of furrows depths (nm). The bars in the histogram correspond to the experimental data and the solid black line corresponds to the fit performed using a log-normal distribution.

Interestingly, the average values obtained from AFC data were systematically lower than those from PF-QNM. This observation can be attributed to the likely viscoelastic properties of the sample[33,34]. In viscoelastic materials, a higher indentation speed, as employed in PF-QNM, can lead to increased resistance during material penetration, resulting in higher measured elastic modulus. Therefore, the AFC data likely provide a more accurate representation of the intrinsic elastic properties of the *S. mansoni* tegument.

Conclusions

The purpose of this work was the morphological and mechanical properties characterization of the helminth *S. mansoni* by Atomic Force Microscopy (AFM). The operating mode used was PeakForce Quantitative Nanomechanical Mapping (PF-QNM), obtaining, thus, original results not found in the literature. With the morphological characterization of female worms, it was possible to analyze the furrows present in their tegument, in particular the depth, whose average value obtained was (128 ± 10) nm. With the characterization of mechanical properties, still without tip calibration in the PF-QNM mode, a pattern of light and dark bands

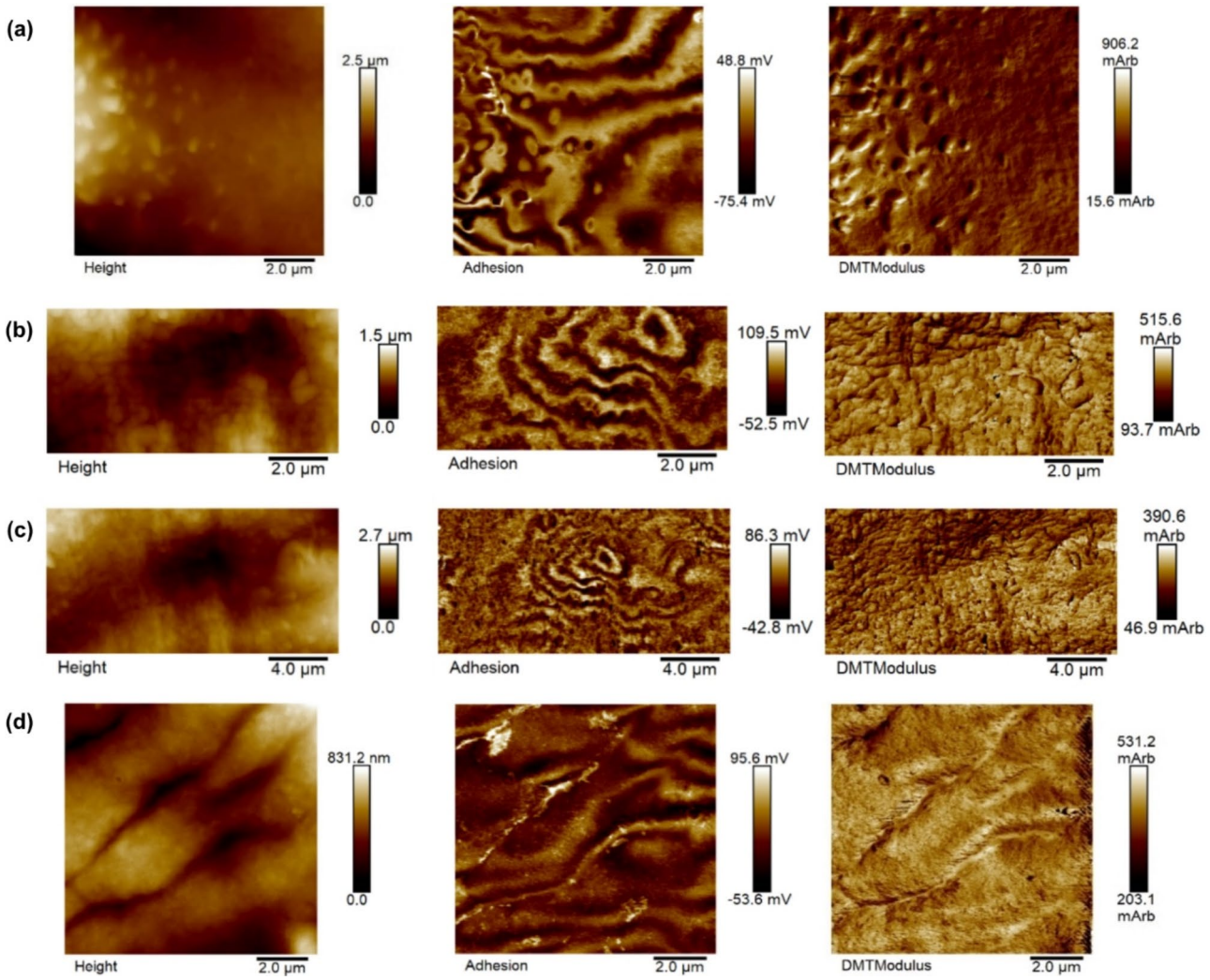

Fig. 5. AFM PF-QNM representative images in air of male *S. mansoni* helminths, regarding topography, adhesion contrast and elastic modulus. Lighter regions in the images indicate areas with higher values of the corresponding property. (**a**) In the topography image, it is noted part of a tubercle with its spicules on one side and smooth regions with no visible structures on the other; images (**b**) and (**c**) correspond to the same region, but with a different scan size and a valley can be seen in the region; (**d**) image of a region between the oral and ventral suckers, its topography reveals furrows.

(fringes) was observed, mainly in the adhesive property image, with an average spatial periodicity of (715 ± 37) nm, although it is not known what produces this pattern.

After tip calibration in PF-QNM mode, images of female worms were obtained, and it was possible to extract and analyze raw force curve data from each image. In parallel to the PF-QNM operating mode, arrays of force curves (AFC) were obtained in AFM contact mode from the same regions as the images obtained by PF-QNM. The force curves were analyzed in a similar way and the elastic modulus of the analyzed regions were obtained for both cases (PF-QNM and AFC). Therefore, it could be inferred that the elastic modulus of the *S. mansoni* helminth is between 0.2 GPa and 3.4 GPa.

In conclusion, the PF-QNM operating mode of AFM demonstrated to be a suitable tool for the characterization of both the topographic and mechanical properties of the *S. mansoni* helminth. Furthermore, the use of the array of force curves in AFM contact mode also demonstrated its effectiveness as an appropriate tool for evaluating the mechanical properties of this helminth. The tegument's role at the parasite-host interface has been extensively studied, revealing its secretory functions, involvement in nutrient absorption, and its ability to shield schistosomes from the host's immune response[35–37]. Additionally, it serves as a primary target for antischistosomal drugs[38,39] Therefore, conducting detailed observations of the tegument's topographic and mechanical properties will deepen our understanding of the host-parasite relationship. This characterization holds significance for future research, facilitating studies on parasite biology and survival under immunological or pharmacological pressure.

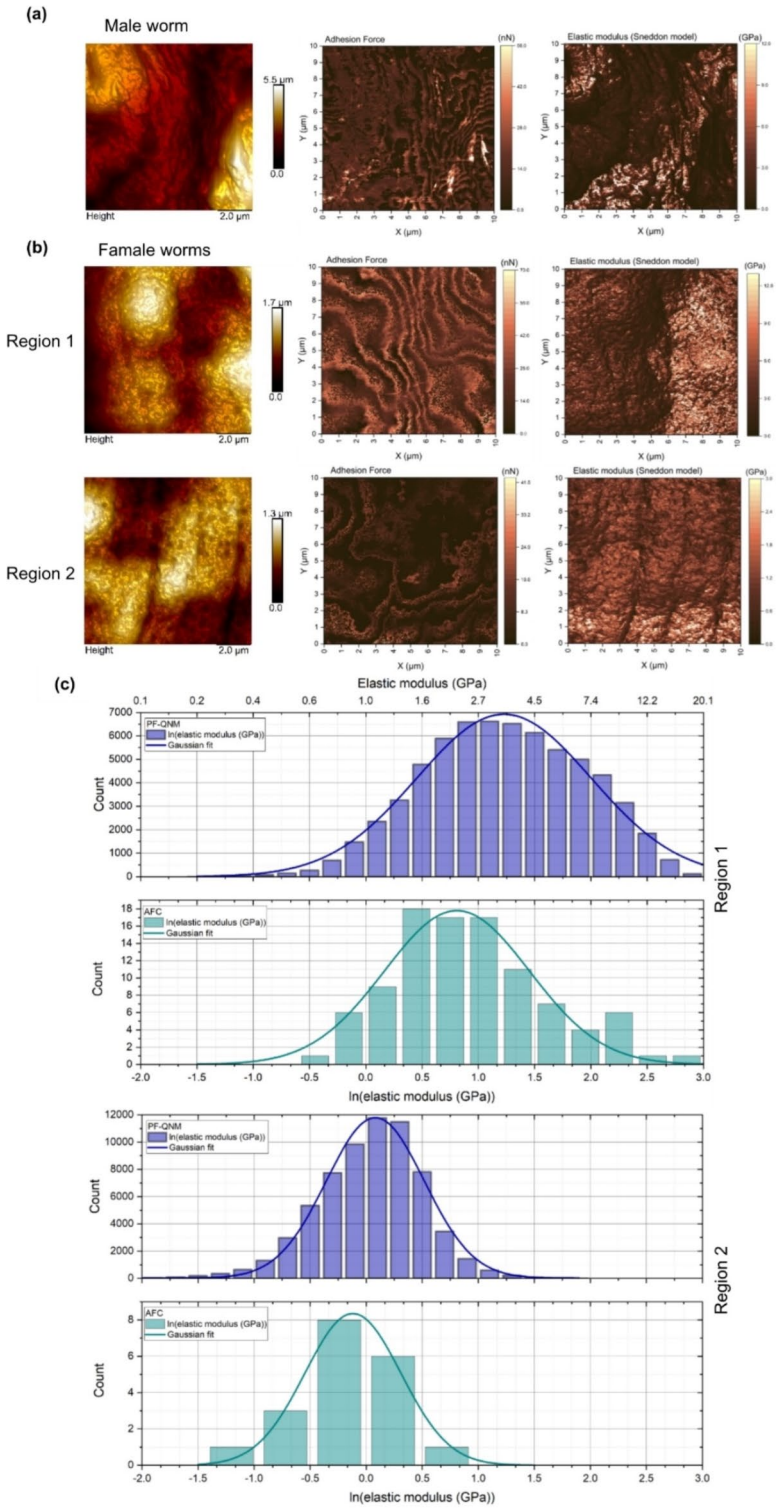

Fig. 6. (**a**) AFM PF-QNM representative images in air of male *S. mansoni* helminth, regarding topography, adhesion contrast and elastic modulus fitted to Sneddon model. (**b**) PF-QNM images of two regions of female worms tegument with contrasts in topography, adhesion, and elastic modulus fitted to Sneddon model; (**c**) Natural logarithm histograms of the elastic modulus (ln(*E*)) of the regions presented in (**b**). The bars correspond to the experimental data and the solid line corresponds to a Gaussian fit. The histograms corresponding to PF-QNM represent 65,536 data, while the histogram corresponding to the array of force curves (AFC) in contact mode of AFM of region 1 represents 100 data, and for region 2 the histogram represents 25 data points. The upper scale of the region 1 histogram corresponds to the value of the elastic modulus in gigapascal (GPa) and serves as a guide for the other histograms.

	Elastic modulus (E) (GPa)		R^2	
	PF-QNM	AFC	PF-QNM	AFC
Region 1	3.42 ± 0.01	2.25 ± 0.26	0.98	0.91
Region 2	1.085 ± 0.002	0.89 ± 0.08	0.99	0.99
Region 3	1.461 ± 0.002	0.38 ± 0.02	0.95	0.90
Region 4	1.099 ± 0.001	0.515 ± 0.009	0.99	0.95
Region 5	1.425 ± 0.002	0.97 ± 0.05	0.99	0.99
Region 6	1.817 ± 0.002	1.04 ± 0.06	0.98	0.91
Region 7	2.73 ± 0.01	0.212 ± 0.003	0.97	0.96

Table 1. Average values of the elastic modulus (*E*) are shown for each region analyzed; the values were obtained from PF-QNM and AFC data with the respective R^2 statistics.

Methods

Maintenance of the S.*mansoni* life-cycle

The life cycle of the *S. mansoni* (Belo Horizonte strain) is maintained in the laboratory by passing it through a snail species, *Biomphalaria glabrata*, serving as an intermediate host, and a mouse, acting as the definitive host, at the Research Center on Neglected Diseases, Guarulhos University, São Paulo, Brazil[40]. Three-week old female Swiss mice were purchased from Animais de Laboratório Criação e Comércio (São Paulo, Brazil). The animals were kept under controlled conditions of temperature (22 °C) and humidity (~ 50%) with *ad libitum* access to water and food. Mice were infected via subcutaneous injection with approximately 120 cercariae, obtained after exposure of snails to light for approximately 3 h. At 42 days post-infection, infected mice were placed in a chamber and euthanized by exposure to 100% medical-grade CO_2, and adult schistosomes were collected from their mesenteric veins.

Sample preparation for Atomic Force Microscopy (AFM)

Adult schistosomes were fixed in AFA solution (70% alcohol, 37% formaldehyde and glacial acetic acid) and carefully placed on the AFM sample holder, which had been prepared beforehand with double-sided tape for secure fixation. Subsequently, the samples underwent a one-hour drying period in an oven set at 37 °C before being transferred for AFM analysis. The samples were left in the AFA fixative for a minimum of 48 h prior to AFM analysis.

Analysis by AFM

The samples were analyzed using a MultiMode 8 SPM microscope (MM-SPM), from Bruker Corporation, using the PeakForce Quantitative Nanomechanical Mapping (PF-QNM)[41] operating mode and force spectroscopy in contact mode, both in air. A probe with a rectangular silicon cantilever (NANOSENSORS NCH-W) was used, with a resonance frequency of 232 kHz. Images were obtained using the PF-QNM mode, initially without tip calibration, with a resolution of 512 × 512 pixels and scan sizes of 5–30 µm. Images were processed using NanoScope Analysis 1.5 software.

The PF-QNM operating mode generates maps of mechanical properties, such as the elastic modulus of the sample and adhesion force between the probe and the sample, together with the three-dimensional topographic image of the surface under analysis. These maps are derived from the analysis of the force curves generated in each pixel of the image, resulting from the interaction between the tip and the sample. To obtain maps of mechanical properties with their usual measurement units, as well as to obtain information on mechanical properties through force spectroscopy, prior tip calibration is necessary[25,42]. Tip calibration is done by obtaining the cantilever deflection sensitivity (unit of nm/V) and probe parameters (tip/cantilever), that are the spring constant of the cantilever and the tip radius. The deflection sensitivity was obtained from a linear adjustment in the contact region of a force curve on a sapphire standard sample (Sapphire-15 M BRUKER PFQNM-SMKit), as shown in Fig. 7. The spring constant of the cantilever was obtained from its thermal fluctuations[43], using the Thermal Tune feature available on the microscope, producing a value of 20 N/m. To measure the tip radius (R), a rough titanium standard sample (RS-15 M BRUKER PFQNM SMKit) was used, which has sharper structures than the AFM tip, allowing to reproduce the image of the extreme tip and with this, the tip radius was measured, and the value of 37 nm was obtained.

When performing a force curve on a sample without any tip calibration, it is generated as shown in Fig. 7a, a graph of the cantilever deflection (in V) as a function of the scanner position (in nm). By obtaining the deflection sensitivity and generating a curve in the sample of interest, we obtain a curve like Fig. 7b (cantilever deflection, in nm, as function of Z position, in nm, of the sample). To obtain the curve in terms of force (in N) as function of Z (in nm), the vertical axis of the curve (in nm) is multiplied by the spring constant (k given by N/m) of the cantilever (Fig. 7c), completing the tip calibration. Therefore, it is noted that the force curves, generated in each pixel, obtained by PF-QNM without tip calibration and by PF-QNM (after tip calibration) differ only by a constant.

After tip calibration, images were collected using the PF-QNM mode with a scan size of 10 µm and a resolution of 256 × 256 pixels. Furthermore, in the same regions imaged with the PF-QNM mode, an array of force curves (AFC) was obtained by force spectroscopy in contact mode. This mode offers the option of obtaining force curves spaced according to the user's previous choice, without, however, generating maps. Note

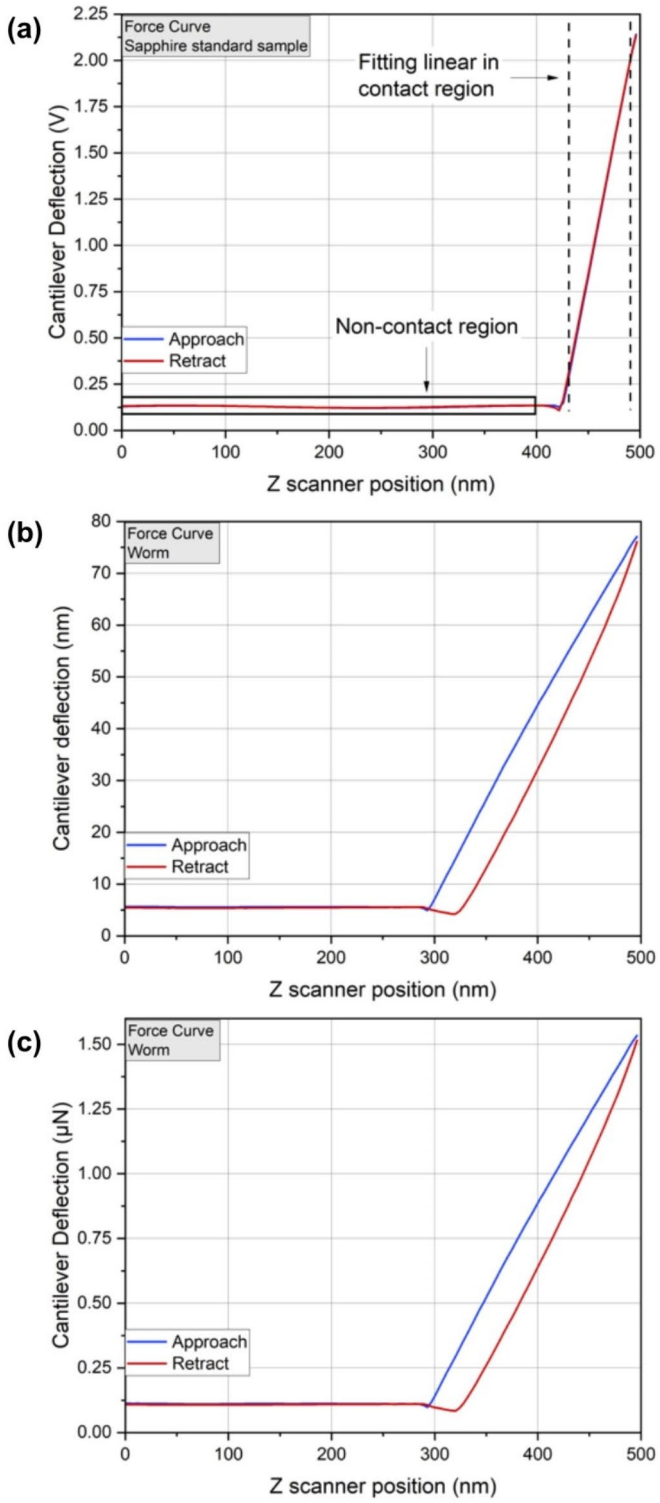

Fig. 7. (**a**) Raw force curve (before tip calibration) of the standard sample (sapphire) to obtain deflection sensitivity. (**b**-**c**) Steps to obtain graph of force as a function of Z position. (**b**) Force curve of worm tegument after obtaining deflection sensitivity. (**c**) Force curve of the worm tegument after obtaining the spring constant.

that, the PF-QNM uses a sinusoidal modulation of the base of the cantilever relative to the sample surface to generate the curves, this controls the normal force of the tip-sample interaction by detecting the peak force of each tap. This sinusoidal waveform causes the tip velocity to approach zero as the tip approaches the peak. On the other hand, single force curves (or AFC) use a linear ramping, where the tip approaches the surface at full

speed. Once the trigger force is detected, the system attempts to retract instantaneously, leading to overshoot and larger forces, especially at higher ramp rates. With this, PF-QNM is able of acquire data in much higher speed[44].

Determination of the elastic modulus

The elastic properties of the sample are determined by fitting a model in the deformation region (also called indentation region) of the force curve, being able to relate the elastic deformation of the sample (δ) to its elastic modulus (also known as Young's modulus). According to the force versus indentation graph, it is possible to assess the elastic and plastic behavior of the sample of interest. A classic model is the Hertz model[45], which considers the adhesion force much smaller than the maximum applied force, that is, $F_{ad} \ll F_{máx}$, and considers the tip indentation in the sample much smaller than the tip radius., that is, $\delta \ll R$.

The model used by PF-QNM to acquire the elastic modulus map is the DMT (Derjaguin-Muller-Toporov) model[46]. This model considers the same conditions as the Hertz model, including the contribution of the adhesion force, which means that the DMT model still considers $\delta \ll R$. In this case, the applied force is given by:

$$F = \frac{4}{3} E_{red} \sqrt{R} \delta^{3/2} - F_{ad} \tag{1}$$

$$\delta = \frac{a^2}{R} \tag{2}$$

where E_{red} is the reduced Young's modulus, R is the tip radius, F_{ad} is the adhesion force, δ is the sample deformation and a is the contact radius between sample tip[41,47].

The raw force curves obtained, both by PF-QNM and AFC, were processed using the AtomicJ software[31] considering the Sneddon model[48] for spherical tips, since our data meet the conditions of this model. The Sneddon model is considered a generalization of the Hertz model, as it can be applied to any tip of arbitrary profile with axial symmetry described as a solid of revolution. The relationship between the applied load, F, and the sample deformation, δ, is given by a transcendental equation that can be computed numerically. For the case of a spherical tip, this relationship is given by the following equations:

$$F = \frac{E_a}{1 - \nu_a^2} \left(\frac{R^2 + a^2}{2} ln \left(\frac{R + a}{R - a} \right) - aR \right) \tag{3}$$

$$\delta = \frac{a}{2} \ln \left(\frac{R + a}{R - a} \right) \tag{4}$$

where E_a is the elastic modulus of the sample and ν_a is the Poisson's ratio of the sample.

Like the Hertz model, the Sneddon model also considers that the adhesion force is much smaller than the maximum applied force, which was compatible with our data. Another condition of the Sneddon model is that the tip indentation in the sample is on the order of the tip radius, i.e., $\delta \sim R$, which is also compatible with our data. For our analyses, Poisson's ratio was considered $\nu_a = 0.5$, as suggested in Hermanowicz et al.[31] for biological samples, and the model was adjusted in the contact region of the approach curve.

Data availability

The raw data that support the findings of this study are available from the corresponding author upon reasonable request.

Received: 8 June 2024; Accepted: 23 September 2024
Published online: 04 October 2024

References

1. WORLD HEALTH ORGANIZATION. Ending the neglect to attain the Sustainable Development Goals: a road map for neglected tropical diseases 2021–2030. (2020).
2. Lago, E. M. et al. Antischistosomal agents: state of art and perspectives. *Future Med. Chem.***10**, 89–120 (2018).
3. WORLD HEALTH ORGANIZATION. Summary of global update on implementation of preventive chemotherapy against NTDs in 2020. (2021).
4. Wiegand, R. E. et al. A persistent hotspot of Schistosoma mansoni infection in a five-year randomized trial of Praziquantel Preventative Chemotherapy Strategies. *J. Infect. Dis.***216**, 1425–1433 (2017).
5. Assaré, R. K. et al. Characteristics of persistent hotspots of Schistosoma mansoni in western Côte d'Ivoire. *Parasites Vectors*. **13**, 337 (2020).
6. Kabuyaya, M., Chimbari, M. J. & Mukaratirwa, S. Efficacy of praziquantel treatment regimens in pre-school and school aged children infected with schistosomes in sub-saharan Africa: a systematic review. *Infect. Dis. Poverty*. **7**, 73 (2018).
7. Spangenberg, T. Alternatives to Praziquantel for the Prevention and Control of Schistosomiasis. *ACS Infect. Dis.***7**, 939–942 (2021).
8. WORLD HEALTH ORGANIZATION & Schistosomiasis (2020). https://www.who.int/news-room/fact-sheets/detail/schistosomiasis
9. Moraes, J. *Efeito in vitro de extratos e Compostos Naturais em Schistosoma mansoni* (Universidade de São Paulo, 2011).
10. Colley, D. G., Bustinduy, A. L., Secor, W. E. & King, C. H. Human schistosomiasis. *Lancet*. **383**, 2253–2264 (2014).
11. McManus, D. P. et al. Schistosomiasis. *Nat. Rev. Dis. Primers*. **4**, 13 (2018).
12. Pinto-Almeida, A. et al. Morphological characteristics of Schistosoma mansoni PZQ-resistant and -susceptible strains are different in presence of Praziquantel. *Front. Microbiol.***7**, 594 (2016).
13. Silva, T. C. et al. New evidence for tamoxifen as an antischistosomal agent: *in vitro*, *in vivo* and target fishing studies. *Future Med. Chem.***13**, 945–957 (2021).

14. Roquini, D. B. et al. Promethazine Exhibits Antiparasitic Properties *In Vitro* and Reduces Worm Burden, Egg Production, Hepatomegaly, and Splenomegaly in a Schistosomiasis Animal Model. *Antimicrob Agents Chemother***63**, e01208-19 (2019).
15. Queiroz, L. S. et al. In vitro and in vivo evaluation of cnicin from blessed thistle (Centaurea benedicta) and its inclusion complexes with cyclodextrins against Schistosoma mansoni. *Parasitol. Res.***120**, 1321–1333 (2021).
16. Moraes, J. D. et al. Schistosoma mansoni: in vitro schistosomicidal activity of piplartine. *Exp. Parasitol.***127**, 357–364 (2011).
17. Veras, M. et al. L. Activity of Epiisopiloturine Against Schistosoma mansoni. *CMC***19**, 2051–2058 (2012).
18. Xavier, A. M. L. et al. Ultrastructural alterations in adult Schistosoma mansoni, harbored in non-antihelminthic treated and low-inflammatory mice by transmission electron microscopy (TEM). *Acta Trop.***130**, 51–57 (2014).
19. Silva, M. P. et al. Antiparasitic activity of nerolidol in a mouse model of schistosomiasis. *Int. J. Antimicrob. Agents*. **50**, 467–472 (2017).
20. Weisberg, L. S., Carlisle, S. & Bentley, A. G. Schistosoma mansoni: evaluation of selected preparative procedures for transmission and Scanning Electron Microscopy. *J. Parasitol.***69**, 335 (1983).
21. Lima, C. et al. Antibacterial, Antibiofilm, and antischistosomal activity of Montrichardia linifera (Arruda) Schott (Araceae) Leaf extracts. *Sci. Pharm.***89**, 31 (2021).
22. Binnig, G., Quate, C. F. & Gerber Ch. Atomic Force Microscope. *Phys. Rev. Lett.***56**, 930–933 (1986).
23. Guo, Q., Xia, Y., Sandig, M. & Yang, J. Characterization of cell elasticity correlated with cell morphology by atomic force microscope. *J. Biomech.***45**, 304–309 (2012).
24. Herrera-Reinoza, N., Junior, T., Teixeira, T. C., Chammas, F. D. S., Salvadori, M. C. & R. & Role of galectin-3 in the elastic response of radial growth phase melanoma cancer cells. *Microscopy Res. Technique*. **86**, 1353–1362 (2023).
25. Oblitas, R. L. D., Camargo Junior, F. B. D., Magalhães, W. V., Sá Teixeira, F. D. & Salvadori, M. C. Characterization of the mechanical properties of the cortex region of human hair fibers by multiparametric atomic force microscopy mapping. *Ultramicroscopy*. **259**, 113925 (2024).
26. Fakhrullina, G., Akhatova, F., Kibardina, M., Fokin, D. & Fakhrullin, R. Nanoscale imaging and characterization of Caenorhabditis elegans epicuticle using atomic force microscopy. *Nanomed. Nanotechnol. Biol. Med.***13**, 483–491 (2017).
27. Pittenger, B., Erina, N. & Su, C. Mechanical property mapping at the Nanoscale using PeakForce QNM scanning probe technique. in Nanomechanical Analysis of High Performance Materials (ed Tiwari, A.) vol **203** 31–51 (Springer Netherlands, Dordrecht, (2014).
28. Brito, J. R. et al. Neolignans isolated from Saururus cernuus L. (Saururaceae) exhibit efficacy against Schistosoma mansoni. *Sci. Rep.***12**, 19320 (2022).
29. Beaux, M. F., Peterson, R. J. & Usov, I. O. Topographic and nanomechanical mapping of plutonium surfaces. *Surf. Interfaces*. **26**, 101382 (2021).
30. Pellegrino, J. & Katz, N. Experimental chemotherapy of Schistosomiasis mansoni. in *Advances in Parasitology*, Vol. 6 (ed. Dawes, B.) 233–290 (Elsevier, 1968).
31. Hermanowicz, P., Sarna, M., Burda, K. & Gabryś, H. AtomicJ: an open source software for analysis of force curves. *Rev. Sci. Instrum.***85**, 063703 (2014).
32. Silva, C. R. et al. Combination of synthetic anthelmintics and monoterpenes: Assessment of efficacy, and ultrastructural and biophysical properties of Haemonchus contortus using atomic force microscopy. *Vet. Parasitol.***290**, 109345 (2021).
33. Efremov, Y. M., Wang, W. H., Hardy, S. D., Geahlen, R. L. & Raman, A. Measuring nanoscale viscoelastic parameters of cells directly from AFM force-displacement curves. *Sci. Rep.***7**, 1541 (2017).
34. Nawaz, S. et al. Cell visco-elasticity measured with AFM and Optical Trapping at Sub-micrometer deformations. *PLoS ONE*. **7**, e45297 (2012).
35. Abath, F. G. C. & Werkhauser, R. C. The tegument of *Schistosoma mansoni*: functional and immunological features. *Parasite Immunol.***18**, 15–20 (1996).
36. Skelly, P. J. & Wilson, R. A. Making sense of the Schistosome surface. in *Advances in Parasitology*, Vol. 63 (eds Baker, J. R. et al.). 185–284 (Elsevier, 2006).
37. Van Hellemond, J. J. et al. Functions of the tegument of schistosomes: clues from the proteome and lipidome. *Int. J. Parasitol.***36**, 691–699 (2006).
38. Xavier, R. P. et al. H1-antihistamines as antischistosomal drugs: in vitro and in vivo studies. *Parasites Vectors*. **13**, 278 (2020).
39. Roquini, V. et al. The Existing Drug Nifuroxazide as an Antischistosomal Agent: *In Vitro*, *In Vivo*, and *In Silico* Studies of Macromolecular Targets. *Microbiol Spectr***11**, e01393-23 (2023).
40. De, J. Antischistosomal Natural Compounds: Present Challenges for New Drug Screens. in *Current Topics in Tropical Medicine* (ed. Rodriguez-Morales, A.)InTech, doi: (2012). https://doi.org/10.5772/27740
41. Bede Pittenger, Erina, N. & Chanmin, S. Quantitative mechanical property mapping at the nanoscale with PeakForce QNM. doi: (2010). https://doi.org/10.13140/RG.2.1.4463.8246
42. Butt, H. J., Cappella, B. & Kappl, M. Force measurements with the atomic force microscope: technique, interpretation and applications. *Surf. Sci. Rep.***59**, 1–152 (2005).
43. Hutter, J. L. & Bechhoefer, J. Calibration of atomic-force microscope tips. *Rev. Sci. Instrum.***64**, 1868–1873 (1993).
44. Pittenger, B. & Slade, A. Performing quantitative nanomechanical AFM measurements on live cells. *Micros Today*. **21**, 12–17 (2013).
45. Hertz, H. Über die Berührung fester elastischer Körper. *Für die reine und angewandte Mathematik.***92**, 156–171 (1881).
46. Derjaguin, B. V., Muller, V. M. & Toporov, Y. P. Effect of contact deformations on the adhesion of particles. *J. Colloid Interface Sci.***53**, 314–326 (1975).
47. Cappella, B. & Dietler, G. Force-distance curves by atomic force microscopy. *Surf. Sci. Rep.***34**, 1–104 (1999).
48. Sneddon, I. N. The relation between load and penetration in the axisymmetric boussinesq problem for a punch of arbitrary profile. *Int. J. Eng. Sci.***3**, 47–57 (1965).

Acknowledgements

This work was supported by *Conselho Nacional de Desenvolvimento Científico e Tecnológico* (CNPq; Grant 305200/2022-4 to MCS and AMCD received a post-graduate fellowship 131692/2021-6) and *Fundação de Amparo à Pesquisa do Estado de São Paulo* (FAPESP; Grant 2023/08418-6 to JM). RAC received a post-graduate fellowship from the Coordenação de Aperfeiçoamento de Pessoal de Nível Superior (CAPES, Finance Code 001). The funding institutions did not have any role in study design, data collection, data analysis, interpretation or writing of the report in this study. Special thanks to Mariana B. Silva for her technical assistance at the *Núcleo de Pesquisa em Doenças Negligenciadas* (Guarulhos University, Brazil).

Author contributions

A.M.C.D., F.S.T., M.C.S., and J.d.M. contributed to conceptualization; A.M.C.D., F.S.T., R.L.O., W.W.R.A., M.C.A., and R.A.C. contributed to experiments and data interpretation; A.M.C.D., F.S.T., M.C.S., and J.d.M. contributed to writing - original draft and visualization; M.C.S., and J.d.M. contributed with resources, writing -

review & editing, project administration, funding acquisition. All authors reviewed the manuscript.

Declarations

Competing interests
The authors declare no competing interests.

Ethical approval
This study was conducted in compliance with the National Centre for the Replacement, Refinement & Reduction of Animals in Research (NC3Rs) ARRIVE guidelines. The experimental protocol was reviewed and approved by the Committee for the Ethical Use of Animals in Experimentation of Guarulhos University (Guarulhos, SP, Brazil; protocol ID 47/20), in accordance with Brazilian law for the Guidelines for Care and Use of Laboratory Animals.

Additional information
Supplementary Information The online version contains supplementary material available at https://doi.org/10.1038/s41598-024-74056-6.

Correspondence and requests for materials should be addressed to J.d.M. or M.C.S.

Reprints and permissions information is available at www.nature.com/reprints.

Publisher's note Springer Nature remains neutral with regard to jurisdictional claims in published maps and institutional affiliations.